JOURNAL OF PROPULSION AND POWER
Vol. 18, No. 6, November–December 2002

Interaction of Decaying Freestream Turbulence with a Moving Shock Wave: Pressure Field

S. Xanthos,* G. Briassulis,† and Y. Andreopoulos‡
City College of the City University of New York, New York, New York 10031

The unsteady interaction of a moving shock wave with nearly homogeneous and isotropic decaying compressible turbulence has been studied experimentally in a large-scale shock-tube facility by using rectangular grids of various sizes. The interaction has been investigated by measuring velocity, total pressure, and temperature inside the flowfield and static pressure at the wall of the shock tube with instrumentation of temporal and spatial resolution. Attenuation of the shock wave strength has been found to take place as a result of the interaction with the turbulent flowfield, which depends on the mesh size of the grid or its Reynolds number, the flow Mach number, and the initial Mach number of the shock wave. Finer grids produce turbulence, which attenuates the shock wave more than coarse grids at the same Mach number. Amplification of pressure fluctuations after the interaction has been observed in all experiments, depending on grid size (initial turbulence level) and shock strength. Furthermore, this amplification is not the same through the whole range of wave numbers resolved.

I. Introduction

TRAVELING shock waves or expansion waves can be generated inside turbines or compressors of turbine engines as a result of unsteady flow phenomena. These moving waves can interact with rotating or stationary blades, as well as with the flow, and may result in phenomena that can affect the operation and performance of the engine. One of these phenomena is the interaction of passing shock waves with turbulence. Of particular interest to those studying turbomachinery is the interaction of traveling shock waves with freestream turbulence, which can be considered as nearly isotropic and nearly homogeneous. In general, interactions of shock waves with turbulent flows are of great practical importance in external or internal aerodynamics of engineering applications because they considerably modify the fluid field by vorticity and entropy production and transport.

Past work that has been recently reviewed by Andreopoulos et al.[1] has shown that the interaction between the shock wave and turbulent flow is mutual and that the coupling between them is very strong. Complex linear and nonlinear mechanisms are involved that can cause considerable changes in the structure of turbulence and its statistical properties and alter the dynamics of the shock wave motion. Amplification of velocity fluctuations and substantial changes in length scales are the most important outcomes of interactions of shock waves with turbulence. This indicates that such interactions may greatly affect mixing. The use of shock waves, for instance, has been proposed by Budzinski et al.[2] as means to enhance mixing of fuel with oxidant in ramjets.

Turbulence amplification through shock wave interaction is a direct effect of the Rankine–Hugoniot relations when they are coupled with the downstream equations. However, this type of amplification should be decoupled from other effects that also contribute to turbulence amplification, such as destabilizing streamline curvature, flow separation, dilatation effects, or longitudinal pressure gradients, which may be present in the flow before or after the interaction with the shock.[3]

The present work focuses on an idealized case of an interaction of a planar shock wave traveling through a grid-generated turbulence. This flow represents an interaction with a simplified yet relevant geometry that can be used to investigate basic physics and/or as a test case for turbulence modeling in computational fluid dynamics. One way to simulate experimentally the aforementioned interaction is by taking advantage of the induced flow behind a moving shock in a shock tube. This flow is passed through a turbulence-generating grid, and the decaying turbulence behind the incident shock interacts with the shock wave after it has been reflected from the end wall of the shock tube. Figure 1a shows a schematic of the flow interaction in the shock tube. This flow configuration in the shock tube provides a platform to investigate some fundamental issues associated with the amplification of turbulence through its interaction with the moving shock wave.

A unique facility has been developed at the City College of the City University of New York (CCNY) in which the Mach number of the flow behind the reflected shock can be controlled independently from the shock wave strength, up to a certain extent. This has been achieved by replacing the end wall of the shock tube with a porous wall of variable porosity. The large size of this facility allows measurements of turbulence with high spatial and temporal resolution (Briassulis and Andreopoulos,[4] Briassulis et al.,[5] and Agui[6]). Thus, shock interactions even with incompressible flows can be generated. Figure 1b depicts the wave patterns generated inside the shock tube and their reflections over various hardware components.

Previous experimental work with this type of shock wave interaction is very limited. Keller and Merzkirch[7] measured the density fluctuations in a similar interaction between a traveling wave and a wake of a perforated plate by using speckle photography. They demonstrated that density fluctuations are considerably amplified. The experimental works of Honkan and Andreopoulos[8] and Honkan et al.[9] mentioned for the first time the effects of the interaction of the shock wave with grid-generated turbulence on the turbulent scales. Haas and Stutervant[10] and Hesselink and Stutervant[11] investigated the interaction of a weak shock wave with a single discrete gaseous inhomogeneity and statistically uniform medium, respectively. It was found that the shock induced Rayleigh–Taylor instability enhances mixing considerably, in that turbulent scales seem to decrease after passage of the shock. The latter is in contrast to previous work by Keller and Merzkirch[7] and Debieve et al.[12] and most probably is due to the Rayleigh–Taylor instability, which is as a result a nonlinear interaction of two preexisting modes in the flow, namely, that of the vorticity mode and that of the entropy.

Received 24 October 2001; revision received 28 April 2002; accepted for publication 20 May 2002.

*Graduate Research Assistant, Experimental Aerodynamics and Fluid Mechanics Laboratory, Department of Mechanical Engineering. Member.

†Graduate Research Assistant, Experimental Aerodynamics and Fluid Mechanics Laboratory, Department of Mechanical Engineering. Member.

‡Professor, Experimental Aerodynamics and Fluid Mechanics Laboratory, Department of Mechanical Engineering. Associate Fellow.

The shock wave from a simplistic point of view can be considered a as steep pressure gradient. Information from experiments and simulation of low-speed flows with such pressure gradients indicate that "rapid distortion" concepts hold and, in the limit of extremely sharp gradients, the nonlinearity may be ignored.[13] The physics associated with the compressibility phenomena that are responsible for this amplification are not well understood.

The first attempt to predict such turbulence amplification is attributed to Ribner.[14,15] His predictions were verified qualitatively by Sekundov[16] and Dosanjh and Weeks.[17] Several analytical and numerical studies of this phenomenon by Morkovin,[18] Zang et al.,[19] Anyiwo and Bushnell,[20] Rotman,[21] Lee et al.,[22] and Hannappel and Friedrich[23] show very similar turbulence enhancement. Chu and Kovasznay[24] indicated that there are three fluctuating modes that are coupled and responsible for the turbulence amplification: 1) acoustic (fluctuating pressure and irrotational velocity mode), 2) turbulence (fluctuating vorticity mode), and 3) entropy (fluctuating temperature mode). These modes are, in general, nonlinearly coupled, and the Rankine–Hugoniot jump conditions across the shock indicate that when any one of the three fluctuating modes is transferred across the shock wave, it not only generates the other two, but it may also considerably amplify itself. The present work focuses on the turbulence and acoustic (pressure) fluctuation mode, because temperature fluctuations are extremely small.[9] We have investigated the transfer of homogeneous and isotropic turbulence across an unsteady normal shock propagating inside the flow. Previous work on this subject is rather limited, if not nonexistant. The reason is that it is rather difficult to experimentally set up a configuration where a decaying, grid-generated turbulence will interact with a plane shock in a wind tunnel. Debieve and Lacharme,[25] for instance, attempted to generate homogeneous and isotropic turbulence by installing a grid inside the settling chamber of a supersonic wind tunnel. The flow, however, became anisotropic after it passed through the contraction of the wind tunnel. In another attempt by Barre et al.[26] to generate shock wave interactions with isotropic turbulence, a normal shock wave was formed by the interaction of two oblique shock waves of symmetrical orientation. However, the flow after the interaction was highly accelerated because of the presence of two shear layers/slip lines at the boundaries of the useful flow region.

The objective of the present research work is a better understanding of the interaction of a moving shock wave with the decaying turbulence. The present work is a continuation of previous experiments that were carried out by Honkan and Andreopoulos[8] and Honkan et al.[9] in a small diameter shock tube as well as by Briassulis et al.[5] in the new high-resolution Shock-Tube Research Facility (STURF) of CCNY. The present paper reports the results of the measurements of the pressure field before and after the interaction with the shock wave. A full description of the incoming compressible decaying turbulence before the interaction can be found by Briassulis et al.[5] Andreopoulos et al. discuss the major conclusions of the shock wave interaction with freestream turbulence in a review.[1]

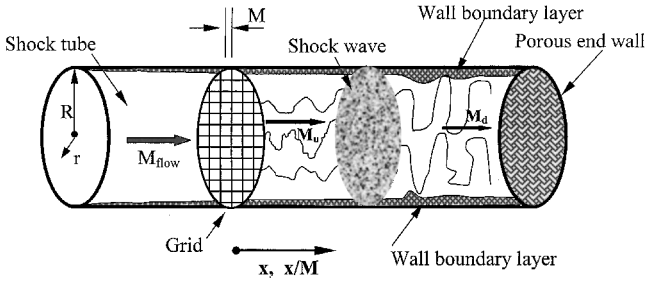

Fig. 1a Schematic of flow interaction.

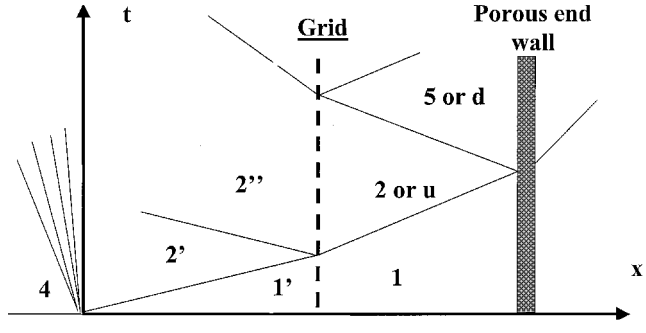

Fig. 1b Interaction *x–t* diagram.

II. New Shock Tube Facility

The experiments were performed in the large-scale STURF, shown in Fig. 2a, which is located at the Mechanical Engineering Department of CCNY. The large dimensions of this facility, 1 ft in diameter and 88 ft in length, provide an excellent platform for high spatial resolution measurements of turbulence with long observation time of steady flow. The induced flow behind the traveling shock wave passes through a turbulence-generating grid installed in the beginning of the working section of the facility. Several turbulence-generating grids were used at four different flow Mach numbers. The velocity of the induced flow behind the shock wave depends on the rupture pressure of the diaphragm, that is, driver strength P_4.

The present shock-tube facility has three distinguishing features. The most significant one is the ability to control the strength of the reflected shock and the flow quality behind it by using a removable porous end wall, placed at the flange between the dump tank and the working section. The impact of shock wave on the end wall would result in a full normal shock reflection in the case of zero porosity (solid wall), a weak shock reflection in case of moderate porosity, or expansion waves in case of infinite porosity (open end wall). The second feature of the facility is the ability to vary the total length of the driven section by adding or removing one of the several pieces or modules that are available or to rearrange their layout. Proper arrangement of the layout of the various modules of the shock tube can maximize the duration of the useful flow. The third feature of the facility is its large diameter, which allows for the availability of a large area of uniform flow in the absence of wall effects, while at the same time providing a platform for high spatial resolution in the measurements of turbulence.

The working (test) section is fitted with several hot-wire and pressure ports (Fig. 2b). Thus, pressure, velocity, and temperature data can be acquired simultaneously at various locations downstream from the grid and, therefore, reduce the variance

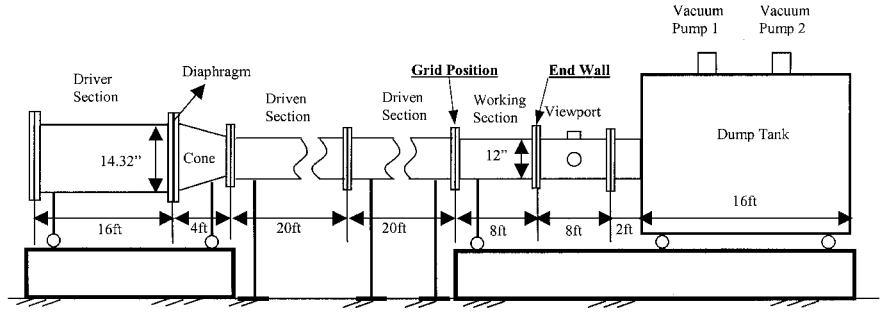

Fig. 2a Schematic of shock tube research facility.

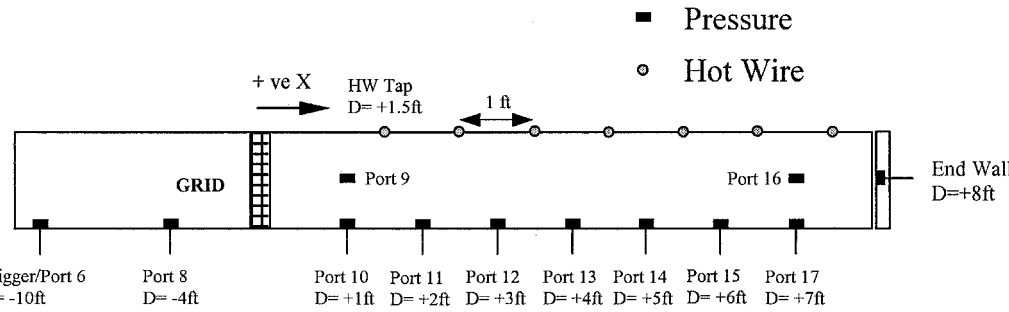

Fig. 2b Two-dimensional schematic of the working section with pressure and hot-wire tap's locations along the 8-ft length.

between measurements. High-frequency pressure transducers, hot-wire anemometry, and Rayleigh scattering techniques for flow visualization have been used in the present investigation. For more details on the hot-wire techniques applicable to shock tubes see Briassulis et al.,[27] who also give estimates of uncertainties in the measurements.

This experimental setup provided simultaneous time-dependent measurements of two velocity components, temperature and wall pressure, at several locations of the flowfield. In addition, time-dependent, three-dimensional vorticity measurements were carried out by using a new vorticity probe (Agui,[6] Briassulis et al.,[5] Andreopoulos and Honkan[28] and Honkan and Andreopoulos[29]).

The shock tube was fitted with nine pressure taps in the working section and eight in the driven section. Pressure transducers were placed throughout the driven section to monitor the passage of the shock wave and also to check its uniformity through the driven section. For the present experiments, high-frequency response Kulite® pressure transducers type XCQ-062 were installed in the shock tube at various locations, so that pressure fluctuations could be measured simultaneously as a function of time. The shock tube was pressurized, so that any leaks could be detected, as well as to calibrate the pressure transducers. The shock tube was free of leaks, and the static response of the transducers was found to be linear. Aluminum plates were used as diaphragms and were placed in between the driver and the conical sections.

A detailed description of the facility and the results of the qualification tests can be found in the work by Briassulis[30] and Briassulis et al.[31]

During each experiment, all signals were acquired simultaneously with the ADTEK data acquisition system. The ADTEK AD830 board is a 12-bit Extended Industry Standard Architecture data acquisition system, capable of simultaneously sampling eight channels at 333 kHz each. Three of those boards are currently available providing 24 simultaneous sampled channels at 333 kHz per channel. Note that no sample-and-hold units were used in the present data acquisition because each channel was dedicated to an individual A/D converter. The data acquisition system was triggered by the arrival of the shock wave at the location of a wall pressure transducer 3.30 m upstream of the grid. The grid was installed in the beginning of the working section.

Several of the experiments were repeated recently by using newly acquired DATEL-416 A/D boards with 1-MHz sampling rate capability and 14-bit resolution. Spectral analysis results, which are shown in this work, are based on data acquired by these high-resolution boards.

The bulk flow parameters of the experiments performed are summarized in Table 1 and include the grid mesh density, the mesh size M, the flow Mach number M_2 behind the incident shock of strength M_s, the Reynolds number based on mesh size Re_M and mean flow velocity U_1, the strength of the reflected shock M_R, and the solidity of the grids σ, defined as the projected solid area per unit total area so that $\sigma = 1 - [1 - d/M]^2$ where d is the rod diameter and M is the mesh size. All grids were fabricated from circular steel rods.

The values of M_2 were obtained in the flow downstream of the grid, and they are slightly smaller than the Mach number values

Table 1 Bulk flow parameters of the experiments performed

Grid, meshes/in.	M, mesh size, mm × mm	Solidity, σ	M_2, flow Mach number	Re_M	Re_λ
10 × 10	2.54	0.36	0.446	40640	N/A
10 × 10	2.54	0.36	0.578	56919	N/A
10 × 10	2.54	0.36	0.6.23	62285	N/A
8 × 8	3.175	0.36	0.371	37138	162
8 × 8	3.175	0.36	0.461	53506	195
8 × 8	3.175	0.36	0.592	63458	246
5 × 5	5.1 × 5.1	0.37	0.371	59654	160–318
5 × 5	5.1 × 5.1	0.37	0.477	86315	200–269
5 × 5	5.1 × 5.1	0.37	0.576	102421	240–458
4 × 4	6.35 × 6.35	0.44	0.354	68208	213–401
4 × 4	6.35 × 6.35	0.44	0.446	105389	198–336
4 × 4	6.35 × 6.35	0.44	0.594	132921	113–352
3 × 3	8.5 × 8.5	0.39	0.321	81687	154–239
3 × 3	8.5 × 8.5	0.39	0.474	124203	184–201
3 × 3	8.5 × 8.5	0.39	0.564	215043	330–747
2 × 2	12.7 × 12.7	0.28	0.346	137319	186–281
2 × 2	12.7 × 12.7	0.28	0.436	169025	195–452
2 × 2	12.7 × 12.7	0.28	0.592	261667	560–1331
1.33 × 1.33	19.05 × 19.05	0.26	0.368	200371	210–278
1.33 × 1.33	19.05 × 19.05	0.26	0.504	295721	217–612
1.33 × 1.33	19.05 × 19.05	0.26	0.607	398661	257–760

obtained in the approaching flow upstream of the grid.[9] As the incoming shock wave reaches the grid, it is transmitted through the grid with some minor losses due to viscous effects, whereas a very weak reflected shock travels as a small disturbance in the opposite direction upstream as a result of the impact of the incident shock on the grid. This disturbance is stronger at higher shock Mach numbers and in impacts with higher solidity grids. This weakly reflected shock reduces the velocity and increases the temperature of the approaching flow by small amounts, respectively. The induced flow behind the incident shock, after it has experienced the effects of the upstream traveling weakly reflected shock, passes through the grid to form a nearly homogeneous and isotropic flow.

III. Shock-Tube Flow

Unlike conventional low-speed grid turbulence, generated in a wind tunnel, the present flow is produced in a shock tube behind a moving shock wave. Shock tubes are traditionally used primarily to study moving shock waves and their reflections or interactions with solid surfaces and to generate high-temperature environments. Our work is not the first to configure a stationary flow behind a moving shock wave. There have been several attempts in the past to utilize the induced flow behind the shock to study several flow phenomena.

The duration of the induced flow behind the shock wave may be limited by the arrival of reflected expansion waves from the driver end wall, which are formed during the rupture of the diaphragm by the arrival of shock or expansion waves formed at the downstream end wall, as well as by the arrival of the contact surface, which is characterized by a large temperature gradient.

The formation of a nearly homogeneous and isotropic turbulent flow with decaying intensity can be described by considering the time-dependent wall pressure signals shown in Fig. 3. The signals

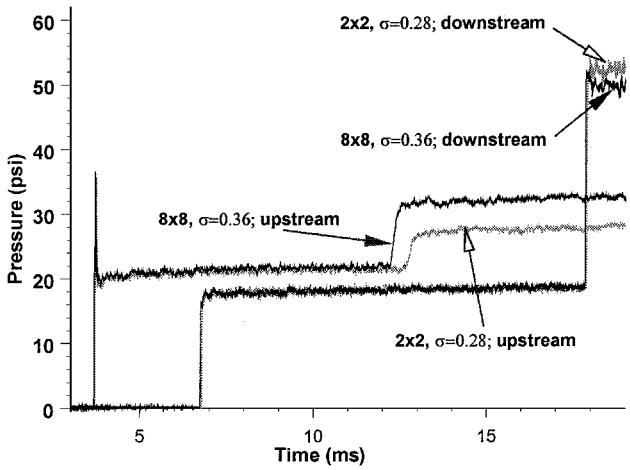

Fig. 3 Time-dependent pressure signals at locations upstream and downstream of grid, $P_4/P_1 = 6.53$.

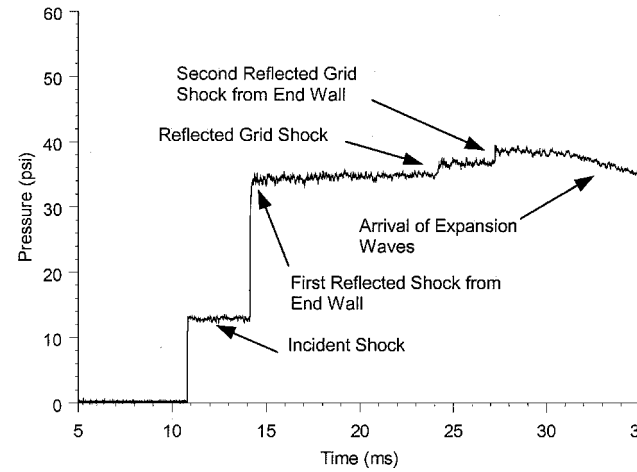

Fig. 4 Typical pressure signal downstream of grid, 5 × 5 grid size, $P_4/P_1 = 4.40$.

shown in Fig. 3 were obtained at two locations, one upstream and one downstream of the grid. Two different grids were used, one with solidity $\sigma = 0.28$ and $M = 12.7$ mm (2 × 2 meshes/in.) and the other with $\sigma = 0.36$ and $M = 3.17$ mm (8 × 8 meshes/in.). The values of pressure plotted in Fig. 3 are above the ambient atmospheric pressure. The incident shock is first detected by the pressure transducer located upstream of the grid. As the incoming shock reaches the grid, it is partly transmitted through the grid with some minor pressure losses associated with viscous effects, it is partly reflected, and it travels in the opposite direction.

This disturbance due to the reflected shock is stronger at higher Mach numbers and in impacts with higher solidity grids. The pressure signals shown in Fig. 3 upstream of the grid correspond to flows with incident shocks of the same strength as those indicated by the same average pressure level behind the grid, yet they clearly demonstrate the effect of grid characteristics on the reflected shock off of the grid. The strength and speed of the reflected shock off of the higher solidity grid (8 × 8) is higher than that in the case of the lower solidity grid (2 × 2).

The reflected shock, which travels in the upstream direction, reduces the velocity and increases the temperature of the approaching flow behind the incident shock by small amounts. The induced flow behind the incident shock, after it has experienced the effects of the upstream-traveling weakly reflected shock, passes through the grid to form a nearly homogeneous and nearly isotropic flow. A full documentation of the velocity field of the decaying turbulence can be found in the work by Briassulis et al.[5]

The minor losses of the transmitted shocks can also be seen in Fig. 3 by considering the pressure signals downstream of the grid location. In general, there some small differences in the level of pressure behind the incident/transmitted shocks, which can be attributed to the different grids. However, in the present case of the 2 × 2 and 8 × 8 grids, the incident shock, after its passage through the grids, has the same strength, to a very good approximation, in both flows.

The incident shock travels downstream and is reflected off of the porous end wall. It then returns to the measuring location after its interaction with the decaying turbulence present in the induced flow behind the incident shock. The pressure signals shown in Fig. 3 show that the arrival of the reflected shock at the measuring location take place at about the same time in both flows. This indicates that both reflected shock fronts travel with the same propagation velocity. The pressure behind them, however, is different, which suggests that the shock strengths are not the same, although their speeds do not differ. One of the objectives of the present research work is to document this behavior and explain its cause.

There are some other issues related to the data processing that need to be discussed in the context of the data statistics presented here. These are demonstrated in Fig. 4, which shows a typical time resolved pressure signal obtained at a location downstream of the grid in an experiment with driver's pressure ratio $P_4/P_1 = 4.4$. P_1 is the pressure in the driven section before the rupture of the diaphragm, which in this particular case was the ambient atmospheric pressure. The signal shows the arrival of the incident shock over the measuring location, followed by the arrival of the reflected shock off of the end wall traveling upstream with Mach number M_R. As this reflected shock reaches the turbulence-generating grid, it is partially transmitted through and is partially reflected in the opposite direction. This reflected grid shock is detected in the measuring location as it travels downstream toward the end wall, where it is reflected and starts traveling in the opposite direction, toward the grid. The pressure signal clearly shows its passage over the location of the pressure transducer.

The pressure signal in Fig. 4 also shows the arrival of the expansion waves, which are formed during the rupture of the diaphragm and that initially travel in the direction opposite the shock wave, toward the end wall of the driver's section, where they are reflected and travel downstream.

Statistical averages were obtained from the quasi-stationary signal before and after the arrival of the reflected shock off of the end wall. The signals were first inspected to detect the presence of undesirable grid shocks or expansion waves within the useful duration of the signals, as well as for their stationarity. Considering the relatively slow growth of the ensemble mean pressure with time verified the stationarity of the data. The reader is referred to Briassulis et al.[5] for a detailed description of the techniques used to obtain reliable statistics from the time-dependent data.

An extensive program has been undertaken to assess the quality of the grid flow established in the shock tube. This was accomplished by measuring the flow uniformity and homogeneity in the working section on planes normal to the flow and in the longitudinal direction. The flow isotropy was also tested and verified by several different methods. Results and details of the flow quality are shown and discussed by Briassulis et al.[5] They have indicated that flow homogeneity is better in fine grids than in coarse ones.

In conclusion, it appears that the quality of the flow established in the shock tube, in terms of uniformity of statistical averages and isotropy, is very good.

IV. Theoretical Considerations

The classical one-dimensional theory describing the unsteady wave patterns in a shock tube with a solid end wall has been extended by Briassulis[30] to include the effects of porosity of the end wall. By solving the equations expressing conservation of mass, momentum, energy, and using the equation of state of the flow behind the reflected shock, one can obtain the pressure and density in this region as a function of the initial conditions. If the mass flux per unit area of the exiting the shock-tube flow behind the reflected shock is $\rho_5 U_5$, and $x = \rho_5 U_5/\rho_2 U_2$, then the strength of the reflected shock

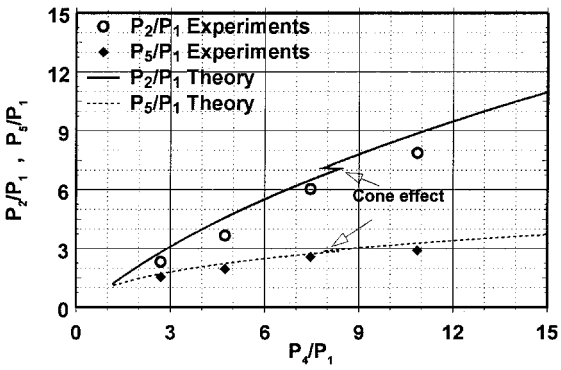

Fig. 5 Comparison of experimental and theoretical data of incident shock strength (P_2/P_1) and reflected shock strength (P_5/P_1) as a function of driver strength $P_4/P_1 = 3.74$.

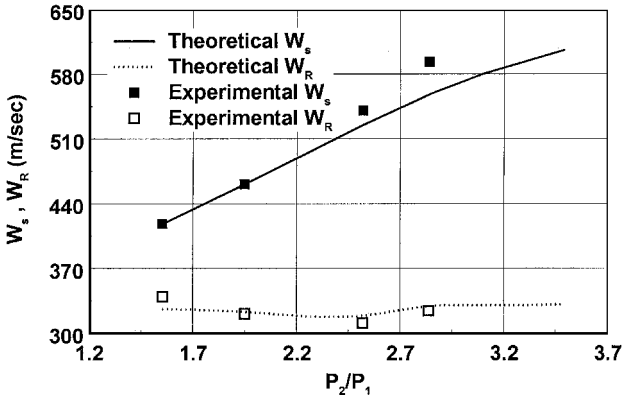

Fig. 6 Comparison between experimental and theoretical shock propagation velocities.

can be obtained from the following equation as a function of M_2 and x:

$$M_R^2 - [(\gamma_1 + 1)/2]M_2(1 - x)M_R - 1 = 0$$

where M_2 the Mach number of the flow behind the incident shock and M_R the Mach number of the reflected shock. The discriminant of this equation is always positive and, therefore, two real solutions are possible. One of the solutions is always negative, and it can be discarded.

Some experimental results are compared with the theoretical calculations without the presence of a turbulence generation grid in Figs. 5 and 6. In particular, in Fig. 5 the driver strength (P_4/P_1) is plotted against the shock strength (P_2/P_1) and reflected shock strength (P_5/P_1). It is obvious that the calculated incident shock strength is in agreement with the experimental shock strength. The same cannot be claimed when the calculated reflected shock strength is compared with the experimental reflected shock strength. The theoretical values are higher than the actual values. There are two reasons for this disagreement. First, the theory developed neglected viscous effects. Second, the flow inside the porous end wall is choked at higher pressure, and, thus, the effective opening area decreases. As a result, the ratio of mass flux exiting the shock tube to the mass flux of the induced flow is less than the mass flux ratio for lower driver strength. Therefore, one reflected shock strength curve cannot accurately describe the whole range of driver strengths.

Figure 6 presents a comparison of the theoretically obtained propagation velocities of the incident and reflected shock, W_s and W_R, respectively, with the experimentally obtained ones for various shock strengths p_2/p_1.

The incident shock velocities seem to agree with the theoretical values at low shock strengths, but at higher shock strengths the theory predicts lower shock velocities, of the order of 10%. It appears that the effect of friction, for the present subsonic cases, on the shock wave speed is greater for the stronger shocks than for the weaker shocks.

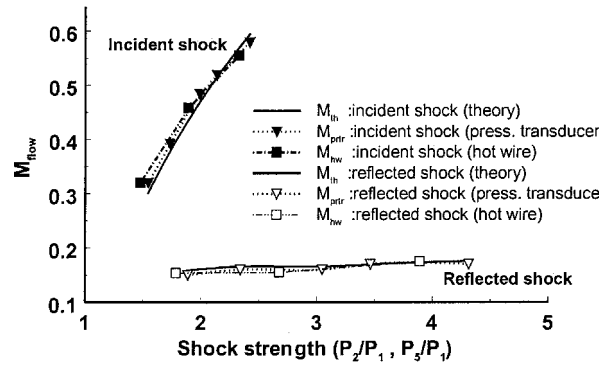

Fig. 7 Comparison of experimental and theoretical mean flow Mach numbers.

The theoretical values of the reflected shock speed W_R agree rather well with the experiments. This suggests that the theory developed here predicts reasonably well the major nonviscous effects involved in the reflection of the shock wave off of the porous end wall.

Hot wires and pressure transducers measured the mean Mach numbers of the flow behind the incident and reflected shock waves in the case of the grid-generated flowfield. These pressure transducers, called Mach probes, were placed inside the flowfield and measured the time-dependent total pressure like pitot tubes. The data obtained by these two techniques are shown in Fig. 7. They are plotted along with the theoretical predictions for several shock strengths of the incident and reflected shocks. It appears that in both cases, incident and reflected, the data agree well with the theoretical predictions. Because the hot-wire measurements and the total pressure measurements were obtained from different experiments, the preceding results confirm the consistency of the experimental techniques, as well as the quality of the flowfield.

V. Results

A. Traveling Shock Waves Through Grids

When a moving shock wave impacts a grid in a face-on fashion, it generates a reflected shock traveling in the opposite direction and a transmitted shock propagating in the same direction as the original shock. (See also the x–t diagram shown in Fig. 1b.) The reflected shock has a higher strength than the incident shock in terms of pressure behind it, whereas the transmitted one has lower strength than the original one. This pressure drop can be expressed in terms of the coefficient K, defined as $K = \Delta p/(1/2\rho U^2)$, where Δp is the difference between the pressure behind the incident shock and the pressure behind the transmitted shock.

This coefficient is expected to be a function of the flow Mach number M_2, the Reynolds number based on the mesh size M, Re_M, and the solidity of the grid σ, that is, $K = K(M_2, Re_M, \sigma)$. Following the work of Laws and Livesey[32] and Groth and Johansson[33] for incompressible flows through fine grids, the dependence of solidity can be isolated from M_2 and Re_M as $K = f(M_2, Re_M)F_\sigma$. Taylor and Davies[34] suggested that the factor F_σ, which, in general, contains the effects of grid geometry, can be expressed in terms of the solidity σ as $F_\sigma = \{[1/(1-\sigma)^2] - 1\}$ because solidity is the dominant geometrical characteristic in the present case. Then, it appears that $K = f(M_2, Re_M)\{[1/(1-\sigma)^2] - 1\}$.

Figures 8a and 8b demonstrate the effects of grid solidity on the transmitted shock wave strength for the 2×2 grid ($M = 12.7$ mm) with $\sigma = 0.28$ and the 4×4 grid ($M = 6.35$ mm) with $\sigma = 0.44$, respectively. Figures 8 show data of the mean pressure distribution along the wall of the working section. The longitudinal distance from the grid has been nondimensionalized by the mesh size M of each grid. In both cases, with the two different grids, the incoming shock wave and flow have the same strength and Mach numbers, respectively. The data in Fig. 8a indicate a pressure drop across

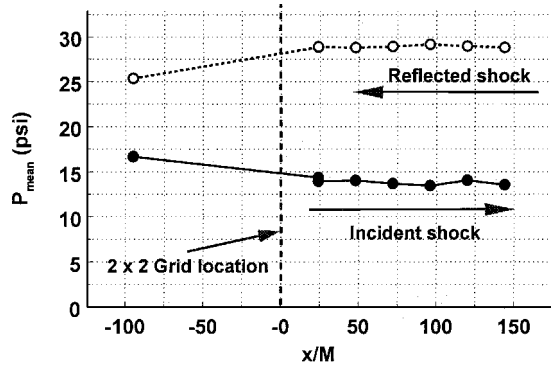

Fig. 8a Mean pressure distribution at $P_4/P_1 = 3.74$ for 2×2 grid.

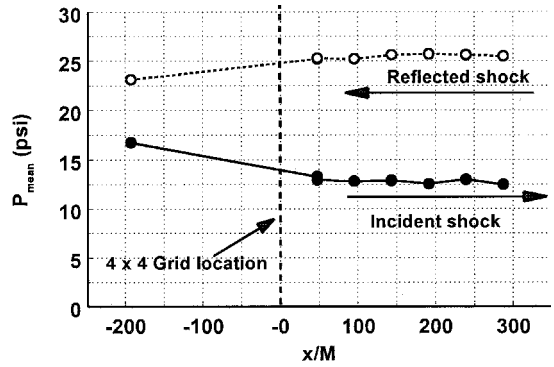

Fig. 8b Mean pressure distribution at $P_4/P_1 = 3.74$ for 4×4 grid.

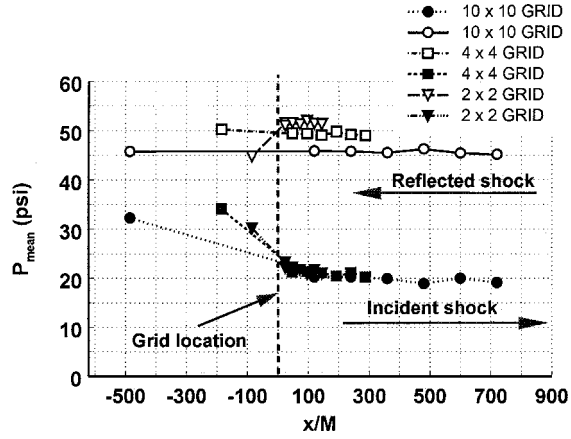

Fig. 9 Mean pressure distribution at $P_4/P_1 = 7.46$ for various grids.

the grid $\Delta p/p$ of about 10%, whereas the corresponding value of F_σ is 0.929. The data in Fig. 8b show a pressure drop, $\Delta P/P$, of about 16% with $F_\sigma = 2.18$. In this particular case, with the same M_2 for both experiments, the function $f(M_2, Re_M)$ depends on Re_M only, that is, $f(Re_M)$. The Re_M for the 2×2 grid is twice the Re_M of the 4×4 grid. According to Pinker and Herbert,[35] the function $f(M_2, Re_M)$ decreases by about 30% for this increase in Re_M.

Thus, the pressure drop coefficient K is expected to be higher in the grid with high solidity by about the ratio (1/1.3) $F_\sigma^{4\times4}/F_\sigma^{2\times2} \cong 1.7$, a value that is close to the experimental data found in the present study.

B. Interaction

The major characteristic feature of the interaction of a shock wave with decaying turbulence is depicted in Fig. 9, where the mean pressure data along the working section are plotted against their normalized distance from the grid location. In all experiments with various grid sizes, the transmitted shock through the grid had the same strength. This was achieved by slightly readjusting the incident shock strength to account for the difference in pressure drops across the various grids, so that the pressure behind the transmitted shock would be practically the same. This way, the shock strength before the reflection off of the end wall and the subsequent interaction with the incoming turbulence was the same in most of these experiments. The data in Fig. 9 show that the pressure downstream of the grid and after the passage of the transmitted shock remains the same in all experiments with the three different grid sizes. The present data also show that the pressure behind the shock does not exhibit any pressure gradient along the working section after the passage of the incident or the reflected shock wave.

Note, in Fig. 9, that the mean pressure behind the reflected shock is not the same in all experiments with the same incident shock strength (P_2/P_1). It appears that the reflected shock strength, P_5/P_1, attenuates more in the case of fine grids. Thus, the pressure jump due to further compression by the reflected shock is less than the value predicted by the inviscid theory. It is obvious that for pressure, there exists a substantial grid dependence, the cause of which has to be further explored.

Three possible explanations have been considered for this behavior. The first one is based on a possibly long-lasting distortion of the shock front, which occurred during its passage through the grid. Numerical simulations have shown that the shock wave is considerably distorted when it is transmitted through the grid. Its front distortion scales with the mesh size M. It is possible that this distortion does not decay quickly and that it has a long-lasting memory. However, experience with shock distortions, based on the experimental and computational results of Xanthos in "Interaction of Grid Turbulence with Expansion or Shock Waves" (Ph.D. Dissertation in preparation) indicates that the shock wave becomes planar within two to three shock-tube diameters after strong reflections over three-dimensional surfaces. In addition, it is rather unlikely that the distorted shock wave retains the grid signature after its reflection off of the end wall of the shock tube.

As a second explanation, the behavior of the present data may be attributed to the different viscous losses occurring during the reflection of the shock in the presence of freestream turbulence. Decaying turbulence generated by the grids is not present during the reflection at the end wall because it travels with the flow speed, which is considerably lower than the speed of the shock wave. Thus, the shock wave and the front of the decaying turbulence cannot be at the end wall location at the same time. The turbulence that is generated inside the unsteady boundary layers developing over the shock tube wall behind the traveling shock and that is present during the reflection has not passed through the grid and, therefore, does not carry any grid signature.

The most plausible interpretation of the present behavior is the strong interaction of the reflected shock wave with the grid-generated turbulent field, which takes place away from the end wall. The first encounter of the reflected shock with the decaying turbulence occurs away from the grid, where the length scales of turbulence are large and the velocity fluctuations are small. As a result of this interaction, the shock wave is distorted considerably by the large eddies of the flow and velocity fluctuations increase as a direct consequence of the Rankine–Hugoniot conditions. Thus, the interaction between the shock wave and the turbulence field appears to be mutual. The shock wave, as it travels through the turbulent flowfield, retains strength, as is evident from the data of mean pressure behind the reflected shock. These data show no substantial pressure gradient (see Fig. 9). It is believed, however, that the majority of the losses of the shock wave's strength occurs in the early stages of the interaction, where the shock front first meets with the front of the decaying turbulence at a location far from the grid and where most of the viscous effects are present. Apparently, these viscous effects are stronger in the case of finer rather than coarser grids. This indicates that the mesh size M, rather than the solidity of the grid, characterizes the interaction.

An attempt has been made to correlate the shock attenuation, expressed as pressure loss ΔP, as a function of the shock Mach number M_r. ΔP is the pressure difference from the corresponding inviscid value predicted by the present theory. The present data,

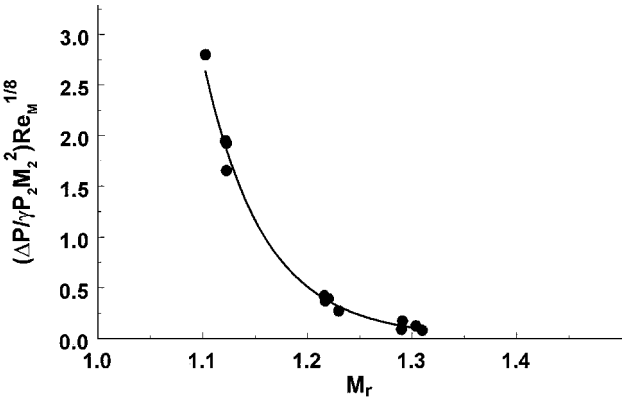

Fig. 10 Shock attenuation vs Mach number of reflected shock M_r.

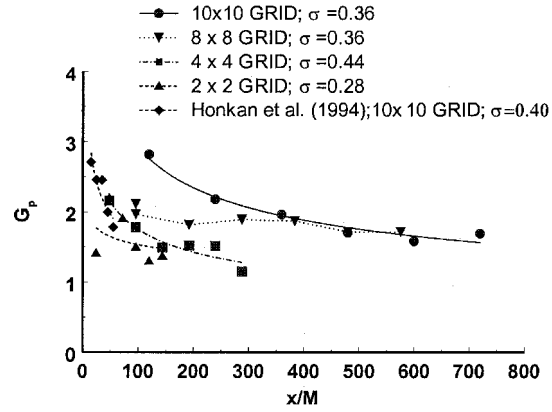

Fig. 12 Amplification of pressure fluctuations for various grids.

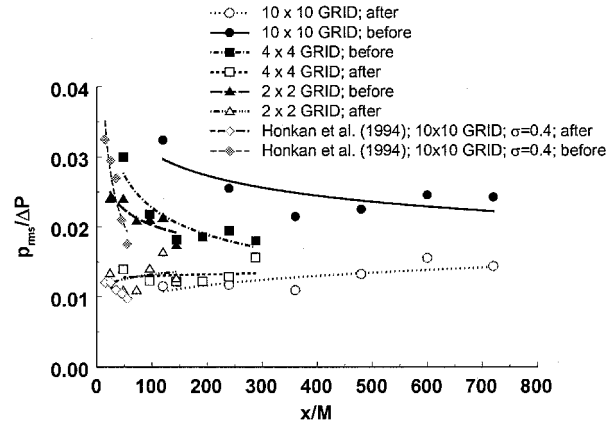

Fig. 11 Pressure fluctuations, rms before and after the interaction for various grids, $\Delta P = P_5 - P_2$: filled symbols, before interaction and open symbols, after interaction.

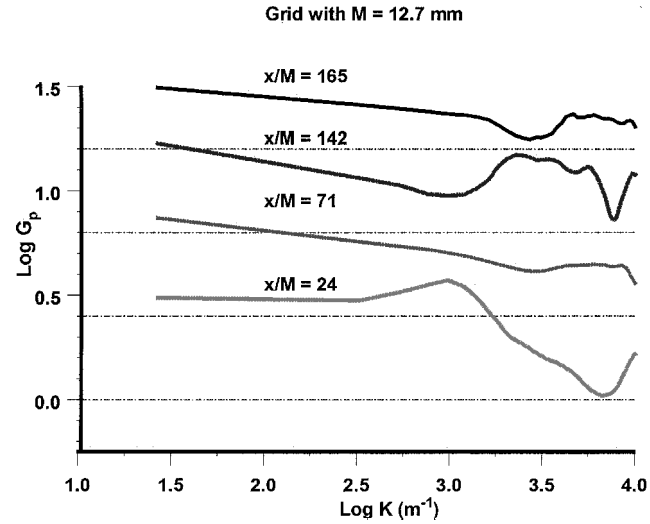

Fig. 13 Amplification of pressure fluctuations G_p, at various wave numbers for the 2 × 2 grid with M = 12.7 mm; data are normalized by the U_2 and U_5.

which are shown in Fig. 10, indicate that the nondimensional shock attenuation $\Delta P/\gamma P_2 M_2^2$ is inversely proportional to $(Re_M)^n$. The best fit of the data resulted in a value of $n = \frac{1}{8}$.

The measured rms data of pressure fluctuations along the flowfield before and after the arrival of the reflected shock wave are shown in Fig. 11. The data have been nondimensionalized by the mean pressure rise across the reflected shock, $P_5 - P_2$. The level of pressure fluctuations before the interaction is between 8 and 15% of the pressure rise due to compression among the data from different grids. After the passage of the shock, the level of pressure fluctuations increases substantially. It appears that the finer the grid, the higher the pressure fluctuations after the interaction.

The amplification factor G_p, defined as the ratio of the rms of pressure fluctuations after the interaction to that before the interaction, is shown in Fig. 12, where the data for three different grids are plotted. Amplification by a factor of 2.8–1.25 can be observed. The data also show that the amplification of pressure fluctuations is not the same through the flowfield. It is higher closer to the grid than it is farther away. Amplification also depends on the grid, that is, more so its mesh size than its solidity. Pressure fluctuations generated by fine grids are amplified more than those generated by coarse grids.

The data of Honkan and Andreopoulos[8] obtained in a different shock tube with 1.75 in. diameter are also plotted in Figs. 11 and 12 for comparison with the present data. They also show amplification ratios similar to the present data.

Amplification of pressure fluctuations at various wave numbers k_n has also been evaluated from the frequency spectra, and it is shown in Fig. 13, where the amplification factor at each wave number is plotted for the 2 × 2 grid ($M = 12.7$ mm). To obtain the wave number spectrum of the pressure fluctuations from the available frequency spectra, the following dispersion relation was used: $\omega - \boldsymbol{u} \cdot \boldsymbol{k} = 0$, where ω is the frequency and k is the wave number vector. This relation is valid under the assumption that vorticity fluctuations are simply advected by the mean flow. In that respect, the mean velocity values before and after the interaction have been used to convert the data from the frequency domain to wave number space.

However, the present flow interaction is caused by the reflected shock moving at constant velocity W_R. Therefore, it may be, appropriate to express the present results on a reference coordinate system moving with the shock. In this case, the relative velocities $W_R + U_2$ and $W_R + U_5$ have been used as convection velocities. The results of this scaling are shown in Fig. 14, where the amplification of pressure fluctuations is shown at different wave numbers. They correspond to the same data obtained with the 2 × 2 grid as the data of Fig. 13.

Had the acoustic mode been solely responsible for the pressure fluctuations present in the flow, then the following dispersion relation, for acoustic waves, would have been used: $\omega - \boldsymbol{u} \cdot \boldsymbol{k} = \pm ck$, where c is the propagation speed of the acoustic wave.[36] Although the acoustic mode is not the dominant one in the present flow, the data of pressure fluctuations at different frequencies have been rescaled to reflect the possibility that they are caused by the acoustic mode. The results are shown in Fig. 15, and they correspond to the same data as in Figs. 13 and 14.

It can be seen from Figs. 13–15 that, in all cases, the amplification is not the same throughout the whole range of wave numbers at a given location. The behavior of high wave numbers appears to be different from that of low wave numbers. Thus, the present data suggest that compression effects on the scales due to shock wave passage are not felt uniformly across the resolved range of scales. In addition, the relative characteristics of the high and low wave numbers also depend on the location.

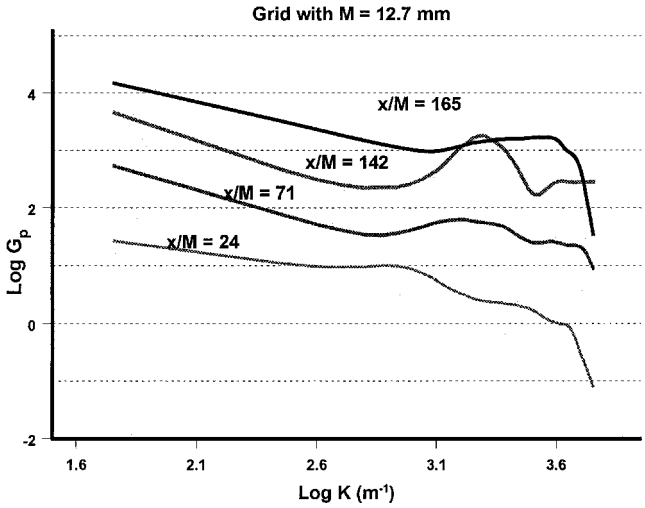

Fig. 14 Amplification of pressure fluctuations G_p, at various wave numbers for the 2 × 2 grid with M = 12.7 mm; data are normalized by $W_R + U_2$ and $W_R + U_5$.

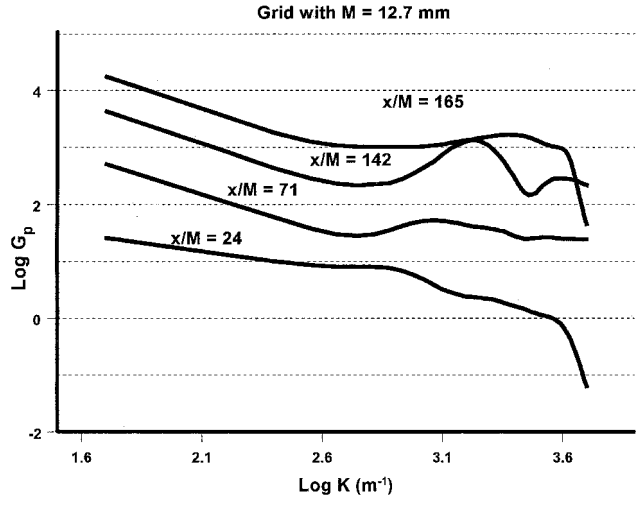

Fig. 15 Amplification of pressure fluctuations G_p, at various wave numbers for the 2 × 2 grid with M = 12.7 mm; data are normalized by $C_2 + U_2$ and $C_5 + U_5$.

Amplification of turbulence has been found in the direct numerical simulations (DNS) of Lee et al.[21] and Hannappel and Friedrich[23] and in the work of Jacquin et al.,[37] which is based on rapid distortion theory. Preferential amplification of turbulence has been also observed in DNS to occur at high wave numbers. In that respect, the present finding is not surprising.

The interpretation of the present results should also be considered in the context of a substantial eddy size growth of the freestream turbulence with downstream distance from the grid, accompanied by a significant decay in turbulence intensity. In addition, wall pressure fluctuations are also caused by the turbulence within the boundary layer developing over the wall. These pressure fluctuations are related to the local shear stress. In fact, Willmarth and Wooldridge[38] and Andreopoulos and Agui[39] found that the rms of pressure fluctuations is about two times the local wall stress. The presence of freestream turbulence increases the local skin friction and, therefore, the wall pressure fluctuations, by roughly 3% for each 1% rms increase in longitudinal intensity (Hancock and Bradshaw[40]). Turbulence intensity of the freestream is between 3 and 7% at distances close to the grid, and it decays to 1% at the last measuring location. These values indicate a 21% increase in pressure fluctuations at locations near the grid and about a 3% increase at locations far away from the grid. The wall stress of the boundary layer, in the absence of freestream turbulence, and, therefore, the rms of pressure fluctuations, is expected to increase slowly with downstream distance. These two counteracting effects seem to explain the slow variation of the rms of pressure fluctuations with distance x/M, before the interaction with the shock wave, shown in Fig. 11. However, the aforementioned is further complicated by the boundary layer flow going through the turbulence-generating grid, and, therefore, it is expected that eddies of the size of the grid mesh size M will be formed. Thus, the reflected shock will interact with a rather complicated boundary-layer turbulence. It appears that the boundary layer responds differently from the freestream region to the new boundary conditions imposed by the wall and the Rankine–Hugoniot conditions imposed by the passing shock. Because the velocity inside the boundary layer is lower than the external velocity, the propagation speed of the reflected shock W_R is higher than the propagation speed in the freestream. The implication is that the reflected shock propagates faster, and it is inclined forward inside the boundary layer. Had the end wall been nonporous, the velocity behind the shock would be zero, and massive separation of the boundary layer would have occurred. The porosity of the end wall imposes a nonzero velocity behind the reflected shock, which improves significantly the overall flow quality in the freestream region. Because the velocity behind the oblique part of the shock and that behind the normal shock do not match in the area around the bending position, a slip line or a better, a shear layer should develop. This flow disturbance is expected to further complicate the flow after the interaction and affect the wall pressure fluctuations. This shear layer is expected to be stronger at locations closer to the end wall, that is, far away from the grid, because of the sharper bending of the reflected shock.

Although the interpretation of the wall-pressure fluctuations data is rather difficult, due to several simultaneously competing phenomena, that the rms of pressure fluctuations after the interaction and the fact their amplification decay with distance downstream of the grid suggests that freestream turbulence appears to play a more dominant role than the other mechanisms discussed.

VI. Conclusions

A nearly isotropic and homogeneous turbulent flowfield was set up in a large-scale shock tube facility by using rectangular grids of various sizes. The induced flow behind the traveling shock, after its passage through the turbulence-generating grid, interacts with the shock wave, which has been reflected off of the porous end wall of the shock tube. This unsteady interaction has been investigated extensively by measuring velocity, total pressure, and temperature inside the flowfield, and static pressure at the wall of the shock tube, with instrumentation of high temporal and spatial resolution.

The interaction between the freestream turbulence and the moving shock wave appears to be mutual. The shock wave strength is attenuated by the interaction due to considerable viscous effects, whereas length scales and the intensity of turbulence change substantially.

The major conclusion of the present study is that the attenuation of the shock wave strength depends on the size of its mesh M or its Reynolds number Re_M, the flow Mach number, and the Mach number of the interacting shock wave. Finer grids produce turbulence, which attenuates the shock wave more than coarse grids at a constant Mach number. The nondimensional parameter attenuation $\Delta P/\rho_2 P_2 M_2^2 (Re_M)^{1/8}$, which characterizes the losses, is reduced in interaction with an increased Mach number of the shock wave.

It was also found that pressure fluctuations are amplified and that their amplification after the passage of the shock wave depends strongly on the grid size for a given shock strength.

The finer grid produces higher-pressure fluctuations on the flowlield. After the interaction of the induced flow with the shock wave, the higher-pressure fluctuations are the ones that are amplified the most.

Spectral analysis of pressure fluctuations indicates different amplification at various wave numbers. Results indicated that the pressure fluctuations associated with large eddies are amplified the most, whereas the pressure fluctuations associated with smaller eddies are not significantly amplified at locations closer to the grid. Far away from the grid, pressure fluctuations associated with smaller eddies are amplified the most.

Acknowledgment

The financial support provided by NASA under Grant NAG-1-1590 is greatly appreciated.

References

[1]Andreopoulos, Y., Agui, J. H., and Briassulis, G., "Shock Wave–Turbulence Interactions," *Annual Review of Fluid Mechanics*, Vol. 32, 2000, pp. 309–345.

[2]Budzinski, J. M., Zukoski, E. E., and Marble, F. E., "Rayleigh Scattering Measurements of Shock Enhanced Mixing," AIAA Paper 92-3546, Jan. 1992.

[3]Andreopoulos, J., and Muck, K. C., "Some New Aspects of the Shock-Wave Boundary Layer Interaction in Compression Ramp Corner," *Journal of Fluid Mechanics*, Vol. 180, 1987, pp. 405–428.

[4]Briassulis, G. K., and Andreopoulos, J., "High Resolution Measurements of Isotropic Turbulence Interacting with Shock Waves," AIAA Paper 96-0042, Jan. 1996.

[5]Briassulis, G. K., Agui, J., and Andreopoulos, Y., "The Structure of Weakly Compressible Grid Turbulence," *Journal of Fluid Mechanics*, Vol. 432, 2001, pp. 219–283.

[6]Agui, J., "Shock Wave Interactions with Turbulence and Vortices," Ph.D. Dissertation, Mechanical Engineering, City Univ. of New York, New York, Sept. 1998.

[7]Keller, J., and Merzkirch, W., "Interaction of a Normal Shock with a Compressible Turbulent Flow," *Experiments in Fluids*, Vol. 8, 1990, pp. 241–247.

[8]Honkan, A., and Andreopoulos, J., "Rapid Compression of Grid-Generated Turbulence by a Moving Shock Wave, *Physics of Fluids A*, Vol. 4, No. 11, 1992, pp. 2562–2572.

[9]Honkan, A., Watkins, C. B., and Andreopoulos, J., "Experimental Study of Interactions of Shock Wave with Free Stream Turbulence," *Journal of Fluids Engineering*, Vol. 116, 1994, pp. 763–769.

[10]Haas, J. F., and Sturtevant, B., "Interaction of Weak Shock Waves with Cylindrical and Spherical Gas Inhomogeneities," *Journal of Fluid Mechanics*, Vol. 181, 1987, pp. 41–58.

[11]Hesselink, L., and Sturtevant, B., "Propagation of Weak Shocks Through Random Medium," *Journal of Fluid Mechanics*, Vol. 196, 1988, pp. 513–53.

[12]Debieve, J. P., and Lacharme, J. P., "A Shock-Wave/Free Turbulence Interaction," edited by J. Delery, Springer-Verlag, Berlin, 1986. pp. 1–14.

[13]Hunt, J. R. C., "A Theory of Turbulent Flow Around Two-Dimensional Bluff Bodies," *Journal of Fluid Mechanics*, Vol. 61, 1973, pp. 625–636.

[14]Ribner, H. S., "Convection of a Pattern of Vorticity Through a Shock Wave," NACA Rept. 2864; also NACA Rept. 1164, June 1953.

[15]Ribner, H. S., "Spectra of Noise and Amplified Turbulence Emanating from Shock–Turbulence Interaction," *AIAA Journal*, Vol. 25, 1986, pp. 436–442.

[16]Sekundov, A. N., "Supersonic Flow Turbulence and Interaction with a Shock Wave," *Izv. Akad. Nauk SSR Mekh. Zhidk. Gaza*, March–April 1974.

[17]Dosanjh, D. S., and Weeks, T. M., "Interaction of a Starting Vortex as well as Karman Vortex Streets with Traveling Shock Wave," AIAA Paper 64-425, Jan. 1964.

[18]Morkovin, M. V., "Note on Assessment of Flow Disturbances at a Blunt Body Traveling at Supersonic Speeds Owing to Flow Disturbances in Free Stream," *Journal of Applied Mechanics*, Vol. 27, 1960, pp. 223–229.

[19]Zang, T. A., Hussaini, M., and Bushnell, D. M., "Numerical Computations of Turbulence Amplification in Shock Wave Interactions," AIAA Paper 82-0293, Jan. 1982.

[20]Anyiwo, J. C., and Bushnell, D. M., "Turbulence Amplification in Shock Wave–Boundary Layer Interaction," *AIAA Journal*, Vol. 20, 1982, pp. 893–899.

[21]Rotman, D., "Shock Wave Effects on a Turbulent Flow," *Physics of Fluids A*, Vol. 3, 1991, pp. 1792–1806.

[22]Lee, L., Lele, S. K., and Moin, P., "Direct Numerical Simulation of Isotropic Turbulence Interacting with a Weak Shock Wave," *Journal of Fluid Mechanics*, Vol. 251, 1993, pp. 533–562.

[23]Hannappel, R., and Friedrich, R., "Direct Numerical Simulation of a Mach 2 Shock Interacting with Isotropic Turbulence," *Applied Science Research*, 1995, 54:205–210.

[24]Chu, B. T., and Kovasznay, L. S. G., "Non-Linear Interactions in a Viscous Heat-Conducting Compressible Flow," *Journal of Fluid Mechanics*, Vol. 3, 1957, pp. 494–514.

[25]Debieve, J. F., and Lacharme, J. P., "A Shock Wave Free-Turbulence Interaction," International Union of Theoretical and Applied Mechanics Conference, 1985.

[26]Barre, S., Allem, D., and Bonnet, J. P., "Experimental Study of Normal Shock/Homogeneous Turbulence Interaction," *AIAA Journal*, Vol. 34, No. 5, 1996, pp. 968–974.

[27]Briassulis, G., Honkan, A., Andreopoulos, J., and Watkins, B. C., "Applications of Hot-Wire Anemometry in Shock Tube Flows," *Experiments in Fluids*, Vol. 19, 1995, pp. 29–37.

[28]Andreopoulos, Y., and Honkan, A., "Experimental Techniques for Highly Resolved Measurements of Rotation, Strain and Dissipation-Rate Tensors in Turbulent Flows," *Measurement Science and Technology*, Vol. 7, 1996, pp. 1462–1472.

[29]Honkan, A., and Andreopoulos, J., "Vorticity Strain-Rate and Dissipation Characteristics in the Near Wall Region of Turbulent Boundary Layers," *Journal of Fluid Mechanics*, Vol. 350, 1997, pp. 29–96.

[30]Briassulis, G. K., "Unsteady Nonlinear Interactions of Turbulence with Shock Waves," Ph.D. Dissertation, Mechanical Engineering, City College of City Univ. of New York, New York, March 1996.

[31]Briassulis, G., Agui, J., Andreopoulos, J., and Watkins, B. C., "A Shock Tube Research Facility for High-Resolution Measurements of Compressible Turbulence," *Experimental Thermal and Fluid Science*, 1996, pp. 430–446.

[32]Laws, E. M., and Livesey, J. L., "A Flow Through Screens," *Annual Review of Fluid Mechanics*, Vol. 10, 1978, pp. 247–266.

[33]Groth, J., and Johansson, A. V., "A Turbulence Reduction in Screen," *Journal of Fluid Mechanics*, Vol. 197, 1988, pp. 139–155.

[34]Taylor, G. I., and Davies, R. M., "The Aerodynamics of Porous Sheets," Aeronautical Research Council, R&M 2237, 1944.

[35]Pinker, R. A., and Herbert, M. V., "Pressure Loss Associated with Compressible Flow Through Square-Mesh Wire Gauzes," *Journal of Mechanical Engineering Science*, Vol. 9, No. 1, 1967, pp. 11–23.

[36]McKenzie, J. F., and Westphal, K. O., "Interaction of Linear Waves with Oblique Shock Waves," *Physics of Fluids*, Vol. 11, No. 3, 1968, pp. 2350–2355.

[37]Jacquin, L., Cambon, C., and Blin, E., "Turbulence Amplification by a Shock Wave and Rapid Distortion Theory," *Physics of Fluids A*, Vol. 5, 1992, pp. 2539–2550.

[38]Willmarth, W. W., and Wooldridge, C. E., "Measurements of the Fluctuating Pressure at the Wall Beneath a Thick Boundary Layer," *Journal of Fluid Mechanics*, Vol. 14, 1962, pp. 187–196.

[39]Andreopoulos, J., and Agui, J., "Wall Vorticity Flux Dynamics in a Two-Dimensional Turbulent Boundary Layer," *Journal of Fluid Mechanics*, Vol. 309, 1996, pp. 45–84.

[40]Hancock, P. E., and Bradshaw, P., "Turbulence Structure of a Boundary Layer Beneath a Turbulent Free Stream," *Journal of Fluid Mechanics*, Vol. 205, 1989, pp. 45–63.